BMC Cancer

RESEARCH

Open Access

An interpretable machine learning model for predicting early liver metastasis after pancreatic cancer surgery

Hao Zhu[1†], Yiyan Zhou[2†], Danyang Shen[1], Kejia Wu[1], Xiaojie Gan[1], Xiaofeng Xue[1], Weigang Zhang[1], Xiaohua Yang[1], Junyi Qiu[1] and Ding Sun[1*]

Abstract

Background Liver metastasis is the most frequent site of distant metastasis in pancreatic ductal adenocarcinoma (PDAC), significantly contributing to poor prognosis. This study aims to develop and validate a machine learning (ML) model for predicting early liver metastasis (ELM) following pancreatic cancer surgery.

Method This retrospective study included 407 pancreatic cancer patients who underwent surgery at the First Affiliated Hospital of Soochow University between January 2015 and December 2023, aiming to develop and validate a predictive model. Seven ML algorithms were employed to predict the risk of liver metastasis within one year after surgery. The training cohort ($n=284$) was used for model development and hyperparameter tuning, while the internal validation cohort ($n=123$) was employed to assess predictive performance. Shapley additive explanations (SHAP) were applied to elucidate the decision-making process of the best-performing model. To assess the generalizability of the model, 131 PDAC patients from the Affiliated Hospital of Nantong University were included as an external validation cohort.

Result A total of 194 patients (36.1%) were diagnosed with ELM during the 1-year postoperative follow-up across the two centers. Out of 22 disease characteristics, nine key features were selected for the development of the model. XGBoost exhibited the highest performance, achieving an AUC of 0.901, accuracy of 0.846, sensitivity of 0.756, specificity of 0.897, and an F1 score of 0.782. The Brier score of 0.12 indicated excellent calibration. Furthermore, both the internal and external validation datasets demonstrated consistent and robust performance, as evidenced by ROC curves, calibration plots, decision curves, and clinical impact curves, thereby supporting its clinical utility.

Conclusion An XGBoost model was developed to predict the likelihood of ELM after PDAC surgery with high accuracy. Additionally, the model was implemented as an application, providing clinicians with an accessible visual tool to support personalized clinical strategies and ultimately enhance patient outcomes.

Keywords Prediction model, Pancreatic cancer, Machine learning, Early liver metastasis, PDAC

†Hao Zhu and Yiyan Zhou contributed equally to this work.

*Correspondence:
Ding Sun
sunding@suda.edu.cn

[1]Department of General Surgery, The First Affiliated Hospital of Soochow University, Suzhou, Jiangsu Province, China
[2]Department of General Surgery, Affiliated Hospital of Nantong University, Nantong, Jiangsu Province, China

Introduction

Pancreatic ductal adenocarcinoma (PDAC) is the most prevalent histological subtype of pancreatic cancer [1]. As one of the leading causes of cancer-related mortality globally, PDAC often presents insidiously, with patients typically diagnosed at advanced stages, and the tumor frequently metastasizing to distant organs [2, 3]. Liver is the most frequent site of distant metastasis in pancreatic cancer; even patients undergoing surgical intervention remain at high risk for postoperative liver metastasis [4]. Currently, standardized methods for predicting early liver metastasis (ELM) after surgery are lacking [5]. Although the existing TNM staging system offers a certain level of risk assessment for PDAC patients [6], its predictive value is constrained by biological variability among individuals. Therefore, there is an urgent need for the development of a non-invasive and accurate predictive model to assess the risk of postoperative liver metastasis in PDAC patients, with the goal of improving prognosis and enabling personalized treatment.

In recent years, machine learning (ML) has gained considerable attention in the healthcare sector, particularly in oncology, owing to its potential to improve the accuracy of predictive models by leveraging large-scale datasets [7]. Previous research has successfully developed machine learning-based predictive models for other metastatic cancers, such as bone metastasis in breast cancer and survival prognosis in tongue cancer, achieving promising outcomes [8, 9]. However, a significant research gap remains in developing predictive models for ELM following pancreatic cancer surgery. To enhance the predictive performance of the model and reduce the dimensionality of the feature space, we employ Lasso regression for feature selection. Lasso regression incorporates an L1 regularization term to penalize less relevant features, effectively selecting key features closely associated with ELM while minimizing the impact of irrelevant or redundant features [10]. We subsequently developed seven ML models, including Logistic Regression (LR), K-Nearest Neighbors (KNN), Random Forest (RF), XGBoost, Decision Tree (DT), Gradient Boosting Machine (GBM), and Support Vector Machine (SVM), to predict ELM outcomes. These models have demonstrated exceptional performance in predicting various clinical outcomes, such as cancer recurrence and metastasis, positioning them as valuable tools in clinical decision-making. However, despite the high accuracy of these ML models, their interpretability remains a major challenge. The "black-box" nature of these models has long hindered their widespread clinical application [11, 12]. To overcome this limitation, the Shapley Additive Explanations (SHAP) method has emerged as a robust framework, providing both global and local explanations for ML predictions. SHAP assigns contribution values to each feature, enabling us to elucidate the impact of each feature on the model's predictions, thereby enhancing the transparency of the decision-making process [13].

Furthermore, we have deployed the XGBoost model, which is the highest-performing predictive model, on an online platform. This overcomes a common limitation in many studies, which develop predictive models without integrating them into practical and accessible platforms [14, 15], thereby improving the model's clinical applicability. The implementation of this approach is of significant value in supporting clinical decision-making, as it allows clinicians to obtain actionable insights into the key factors influencing the model's predictions, thereby facilitating more accurate medical decisions.

Methods and materials

Patients

This study aims to develop and validate a predictive model for ELM in PDAC. We retrospectively collected clinical data from 407 PDAC patients who underwent surgery at the First Affiliated Hospital of Soochow University between January 2015 and December 2023. These data were utilized as the training and internal validation cohorts. Additionally, clinical data from 131 PDAC patients who underwent surgery at the Affiliated Hospital of Nantong University between January 2018 and December 2023 were included as the external validation cohort. All patients underwent standard pancreatic cancer surgeries with pathological confirmation and met the established diagnostic criteria for PDAC. The inclusion criteria were as follows: (1) pathologically confirmed PDAC with a clinical diagnosis consistent with imaging findings (e.g., CT, MRI); (2) surgical treatment for pancreatic cancer, with regular postoperative imaging or percutaneous biopsy within one year to assess the presence of ELM; (3) no development of other malignancies or significant diseases during the follow-up period. The exclusion criteria were: (1) prior radiotherapy, chemotherapy, or other malignancy treatments before surgery; (2) patients with distant metastasis at diagnosis; (3) patients with significant missing clinical data or those unable to undergo subsequent follow-up.

Data collection

Data were extracted from the HAITAI Electronic Medical Record System (Version 4.0) for PDAC patients admitted to the hospital. The following variables were included: (1) demographic information, including gender, age, and body mass index (BMI); (2) laboratory test results obtained within one week prior to surgery, including white blood cells (WBC), red blood cells (RBC), hemoglobin (Hb), platelets (Plt), albumin (Alb), and tumor markers such as CA199, CEA, AFP, and CA125; (3) pancreatic cancer-related tumor characteristics,

including tumor location, size, differentiation, presence of tumor embolism, nerve invasion, and staging information (T-stage, N-stage); (4) other patient conditions, including the presence of fatty liver disease, liver function according to the Child-Pugh classification, and whether postoperative chemotherapy was administered.

Data analysis and methodology

In this study, the baseline characteristics of patients were described and compared separately for continuous and categorical variables. The normality of continuous variables was assessed using the Kolmogorov-Smirnov test. If the variables followed a normal distribution, they were expressed as mean ± standard deviation ($\bar{x} \pm s$) and compared between groups using independent samples t-tests. For variables that did not follow a normal distribution, they were described as median (interquartile range, IQR) and compared using the Mann-Whitney U test. Categorical variables were presented as frequencies and percentages, with differences between groups assessed using Pearson's chi-square test. Data analysis was performed using R software (version 4.3.2) and SPSS (version 25.0), which included processing and validation of the training set, internal validation set, and external validation set. All tests were two-tailed, with a p-value of < 0.05 considered statistically significant. Data processing was conducted in strict adherence to medical statistical standards to ensure the scientific validity and reliability of the results.

To ensure the generalizability of the model, the dataset was randomly divided into a training set and an internal validation set in a 7:3 ratio. In the feature selection process, univariate analysis was first performed to evaluate the relationship between each feature and the outcome variable, facilitating the preliminary identification of potentially significant features. Subsequently, Lasso regression with L1 regularization was applied to further refine the feature space, prioritizing features with higher predictive value while eliminating unnecessary or redundant features. Finally, multivariate analysis was conducted to combine and validate the selected features, ensuring their significance and stability under multidimensional interactions.

This study develops predictive models based on seven ML algorithms: LR, KNN, RF, XGBoost, DT, GBM, and SVM. Feature variables were selected using the previously described feature selection methods. The feature data were standardized using the preProcess function to mitigate the impact of varying scales on model training. Subsequently, 10-fold cross-validation was applied to ensure the stability of data partitioning and the reliability of the results. Hyperparameter optimization was conducted through grid search, selecting the combination of hyperparameters that maximized the area under the receiver operating characteristic (AUC). The AUC, accuracy, sensitivity, specificity, and F1-score of each model were computed on the validation set to assess overall model performance and identify the best-performing model. Further analysis was performed using ROC curves, Precision-Recall curves, Calibration curves, and Decision Curve Analysis (DCA) to evaluate classification performance and stability of the seven models at various thresholds [16]. Finally, the generalizability and clinical applicability of the best model were validated in the training, internal validation, and external validation sets using ROC curves, calibration curves, decision curves, and clinical impact curves (CIC). Visualization tools, including SHAP Summary Plots, SHAP Bar Plots, SHAP Dependence Plots, and individual sample force plots, were used to display the global importance of each feature and its contribution to individual predictions. Ultimately, a clinical application platform was developed to translate the research findings into a practical tool for clinical use. The various steps of this study are depicted in Fig. 1.

Result

Handling of missing values

This study incorporated data from 23 variables, with 112 missing values, representing 1.19% of the total dataset. The missing data were predominantly linked to the Child-Pugh score, WBC, RBC, Hb, PLT, Alb, CA199, CEA, AFP, and CA125. Among these variables, CA125 exhibited the highest proportion of missing data, accounting for 0.38% of the entire dataset. No missing data were observed in the remaining variables (Figure S1). The majority of missing values arose from updates to the inpatient electronic medical record system (e.g., system version upgrades or incomplete data migration), while a smaller portion stemmed from incomplete examination records, which hindered data collection. Missing values were imputed using the K-Nearest Neighbors (KNN) imputation method to minimize their potential impact on model development.

Baseline characteristics of patients

From January 2015 to December 2023, a total of 407 patients with PDAC were treated at the Department of Hepatobiliary and Pancreatic Surgery, First Affiliated Hospital of Soochow University. Of these, 259 patients did not develop liver metastases within one year post-surgery, whereas 148 patients were diagnosed with ELM within one year based on imaging or biopsy pathology. Patients were randomly assigned to a training set and an internal validation set in a 7:3 ratio. Table 1 compares patients with and without liver metastases in the training and internal validation sets, showing significant differences in BMI, fatty liver, Child-Pugh score, tumor location, size, T stage, N stage, differentiation,

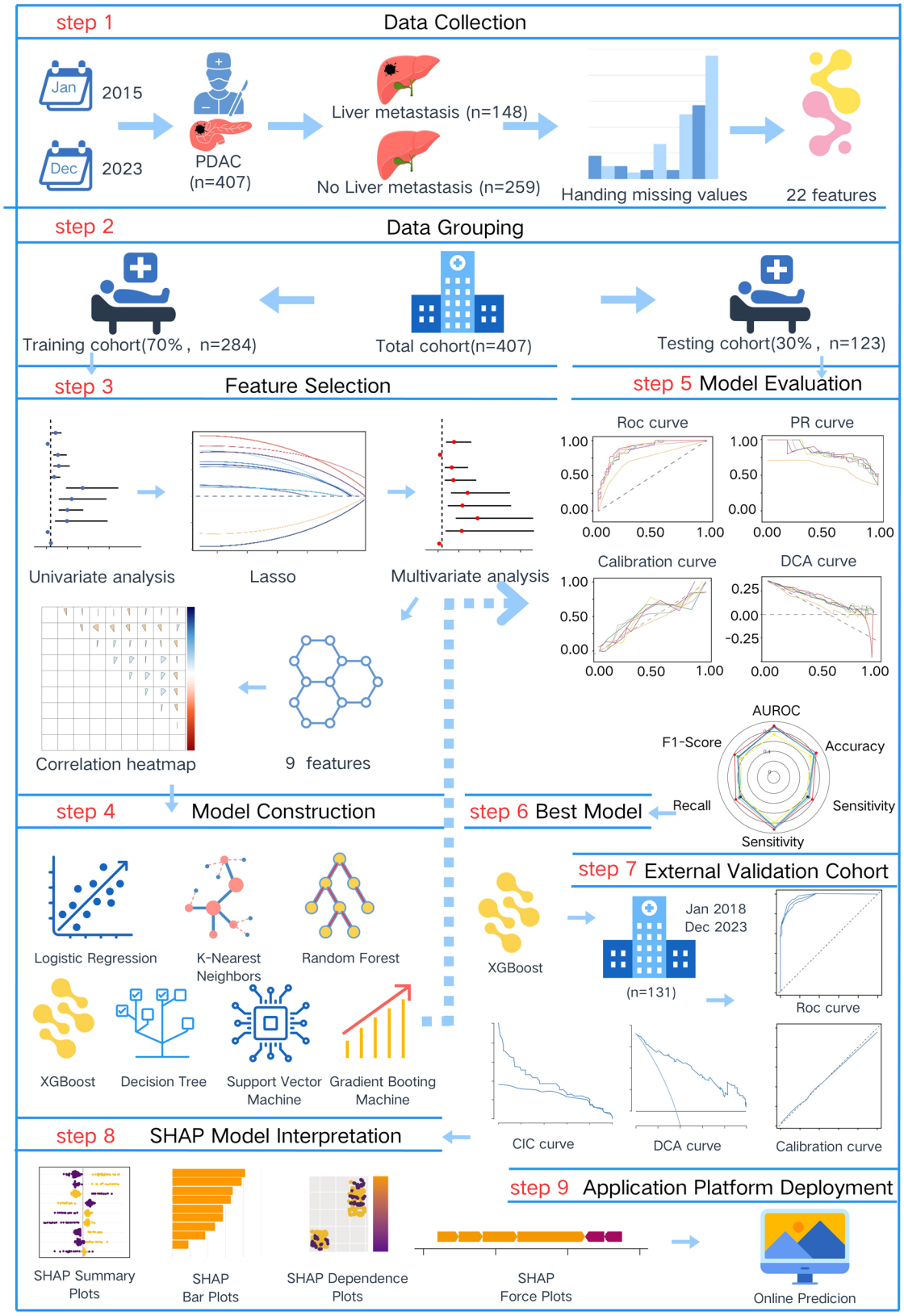

Fig. 1 Flow diagram of the predictive model

Table 1 Clinical characteristics of PDAC and ELM patients in the training and internal validation cohorts

Characteristics	Training cohort			Internal validation cohort		
	PDAC (*n* = 181)	ELM (*n* = 103)	*p*. value	PDAC (*n* = 78)	ELM (*n* = 45)	*p*. value
Age			0.93			0.479
< 60	73(40.3%)	33(32%)		31(39.7%)	15(33.3%)	
≥ 60	108(59.7%)	70(68%)		47(60.3%)	30(66.7%)	
Gender			0.07			0.164
Male	108(59.7%)	50(48.5%)		42(53.8%)	30(66.7%)	
Female	73(40.3%)	53(51.5%)		36(46.2%)	15(33.3%)	
BMI			0.006			0.015
< 24	140(77.3%)	64(62.1%)		64(82.1%)	28(62.2%)	
≥ 24	41(22.7%)	39(37.9%)		14(17.9%)	17(37.8%)	
Fatty liver			< 0.001			0.008
No	102(56.4%)	89(86.4%)		42(53.8%)	35(77.8%)	
Yes	79(43.6%)	14(13.6%)		36(46.2%)	10(22.2%)	
Child-Pugh			< 0.001			<0.001
A	150(82.9%)	66(64.1%)		68(97.2%)	23(51.1%)	
B	31(17.1%)	37(35.9%)		10(12.8%)	22(48.9%)	
ALB(g/L)			0.768			0.712
< 35	36(19.9%)	22(21.4%)		16(20.5%)	8(17.8%)	
≥ 35	145(80.1%)	81(78.6%)		62(79.5%)	37(82.3%)	
Location			< 0.001			0.005
Head	63(34.8%)	16(15.5%)		29(37.2%)	6(13.3%)	
Body and Tail	118(65.2%)	87(84.5%)		49(62.8%)	39(46.7%)	
T. stage			0.045			0.012
T1-2	150(82.9%)	75(72.8%)		63(80.8%)	27(60%)	
T3-4	31(17.1%)	28(27.2%)		15(19.2%)	18(40%)	
N. stage			< 0.001			<0.001
N0-1	166(91.7%)	58(56.3%)		71(91%)	28(62.2%)	
N2	15(8.3%)	45(43.7%)		7(9%)	17(37.8%)	
Differentiation			< 0.001			0.002
G1-2	61(33.7%)	8(7.8%)		27(34.6%)	4(8.9%)	
G3-4	120(66.3%)	95(92.2%)		51(65.4%)	41(91.1%)	
Tumor embolus			< 0.001			<0.001
No	152(83.9%)	53(51.5%)		62(79.5%)	21(46.7%)	
Yes	29(16.1%)	50(48.5%)		16(20.5%)	24(53.3%)	
Nerve invasion			0.001			0.058
No	36(19.9%)	5(4.9%)		15(19.2%)	3(6.7%)	
Yes	145(80.1%)	98(95.1%)		63(80.8%)	42(93.3%)	
Adjuvant chemotherapy			< 0.001			0.053
No	31(17.1%)	47(45.6%)		14(17.9%)	15(33.3%)	
Yes	150(82.9%)	56(54.4%)		64(82.1%)	30(66.7%)	
Wbc	5.64 [4.64; 7.31]	5.58 [4.36; 6.6]	0.546	5.35 [4.75; 7.32]	5.31 [4.47; 7.1]	0.556
Rbc	4.14 [3.68; 4.4]	4.01 [3.5; 4.24]	0.167	4.095 [3.64; 4.45]	4.12 [3.68; 4.39]	0.783
Hb	125 [112; 133]	123 [111; 130]	0.099	123 [111.25; 132.75]	124 [116; 129]	0.864
Plt	194 [157; 222]	199 [165; 231]	0.105	197 [170; 244]	202 [165; 251]	0.992
Ca199	345 [59.22; 1200]	299.15 [88.16; 844.78]	0.392	488.36 [89.26; 1075.56]	488.36 [46.38; 1200]	0.983
CEA	3.72 [2.3; 5.72]	4.27 [2.75; 6.18]	0.369	4.64 [2.38; 6.8]	3.72 [2.19; 5.62]	0.263
AFP	2.55 [2; 3.22]	2.48 [2; 3.24]	0.863	2.2 [2; 2.81]	2.29 [2; 2.71]	0.754
Ca125	20.2 [13.3; 32.5]	20.2 [13.05; 34.35]	0.942	20.3 [14.6; 34]	20.2 [15.2; 30.4]	0.966
Tumor size	3[2.5; 4.0]	3.5[3.0; 4.2]	0.024	3 [2.5; 4]	4 [3; 5]	0.008

ALB Albumin, *Wbc* White blood cell, *Rbc* Red blood cell, *Hb* Hemoglobin, *Plt* Platelet, *Ca199* Carbohydrate Antigen 199, *CEA* Carcinoembryonic Antigen, *AFP* Alpha-Fetoprotein, *Ca125* Carbohydrate Antigen 125

tumor embolus, nerve invasion and adjuvant chemotherapy ($p < 0.05$). Importantly, among the 300 patients who received postoperative chemotherapy, 148 (49.3%) were treated with gemcitabine/nab-paclitaxel (GA), 113 (37.7%) with FOLFIRINOX, and 39 (13.0%) with other regimens due to toxicity or disease progression. The ELM rates were 46 cases (31.1%) in the GA group, 28 cases (24.8%) in the FOLFIRINOX group, and 12 cases (30.8%) in the other group ($p = 0.511$), indicating no significant impact of chemotherapy regimen on metastatic outcomes. These patients were evenly distributed between the training set (99 GA, 82 FOLFIRINOX, 25 other) and validation set (49 GA, 31 FOLFIRINOX, 14 other) ($p = 0.498$). Table S1 summarizes the baseline characteristics of the two datasets, indicating no significant differences between the groups ($p \geq 0.05$). The external validation cohort included 85 non-metastatic and 46 metastatic patients treated at the Affiliated Hospital of Nantong University between January 2018 and December 2023. Baseline characteristics are summarized in Table 2.

Feature selection in predictive modeling

A univariate logistic regression analysis was conducted on all candidate variables, with a threshold of $p < 0.05$ for selection, identifying BMI, fatty liver, Child-Pugh score, tumor location, T stage, N stage, differentiation, tumor emboli, nerve invasion, adjuvant chemotherapy, and CEA as significant predictors (Fig. 2A). These variables were deemed potential predictors and were incorporated into subsequent analyses.

Lasso regression was applied to further refine the feature set, utilizing the second optimal penalty parameter (λ) within one standard error of the minimum mean squared error to strike a balance between model simplicity and predictive performance. The analysis revealed that the regression coefficient for T stage was reduced to zero, leading to its exclusion from the model (Fig. 2B, C, Table S2). The remaining variables were retained for multivariate logistic regression analysis, with CEA excluded due to a lack of statistical significance ($p > 0.05$) (Fig. 2D).

To ensure the independence of variables, multicollinearity was assessed for those retained after the multivariate analysis. Variance inflation factor (VIF) and tolerance were calculated, with thresholds of VIF > 5 or tolerance < 0.1 set for exclusion. The results showed no significant multicollinearity among the variables (Figure S2). Ultimately, nine variables—BMI, fatty liver, Child-Pugh score, tumor location, N stage, differentiation, tumor emboli, nerve invasion, and adjuvant chemotherapy—were retained for model development. Further analysis revealed that the correlation coefficients between these variables were low, confirming their independence (Fig. 3).

Table 2 Clinical characteristics of PDAC and ELM patients in the external validation cohort

Characteristics	External Validation Cohort		*p*. value
	PDAC	ELM	
	N = 85	*N* = 46	
Gender			0.319
Male	52(61.2%)	24(52.2%)	
Female	33(38.8%)	22(47.8%)	
Age			0.335
< 60	35(41.2%)	15(32.6%)	
≥ 60	50(58.8%)	31(67.4%)	
BMI			0.24
< 24	62(72.9%)	29(63.1%)	
≥ 24	23(27.1%)	17(36.9%)	
Fatty liver			<0.001
No	43(50.6%)	39(84.8%)	
Yes	42(49.4%)	7(15.2%)	
Child-Pugh	.	.	0.006
A	73(85.9%)	30(65.2%)	
B	12(14.1%)	16(34.8%)	
Alb			0.604
< 35	18(21.2%)	8(17.4%)	
≥ 35	67(78.8%)	38(82.6%)	
Location			0.08
Head	29(34.1%)	9(19.6%)	
Body and Tail	56(65.9%)	37(80.4%)	
T.stage			0.001
T1-2	76(89.4%)	30(65.2%)	
T3-4	9(10.6%)	16(34.8%)	
N.stage			<0.001
N0-1	76(89.4%)	24(52.2%)	
N2	9(10.6%)	22(47.8%)	
Differentiation			<0.001
G1-2	26(30.6%)	1(2.17%)	
G3-4	59(69.4%)	45(97.8%)	
Vascular embolism			<0.001
No	71(83.5%)	23(50%)	
Yes	14(16.5%)	23(50%)	
Nerve invasion			<0.001
No	18(21.2%)	2(4.3%)	
Yes	67(78.8%)	44(95.7%)	
Adjuvant chemotherapy			0.004
No	14(16.5%)	18(39.1%)	
Yes	71(83.5%)	28(60.9%)	
Wbc	5.64 [4.47; 7.48]	5.875 [4.42; 7.82]	0.7484442
Rbc	4.13 [3.68; 4.44]	4.06 [3.6; 4.2]	0.2214396
Hb	124 [112; 136]	119 [109.5; 128.5]	0.0983594
Plt	194 [163; 229]	198 [162.75; 260]	0.2746742
Ca199	412.98 [79.27; 1075.56]	577.385 [87.08; 1200]	0.6733674
Cea	4.4 [2.63; 5.76]	4.4 [2.81; 5.92]	0.8906787
Afp	2.48 [2; 3.09]	2.43 [2; 3.06]	0.8882542
Ca125	22.7 [14.9; 36.2]	20.7 [13.7; 44.3]	0.9078537
Size	3 [2.5; 3.5]	4 [3; 4.5]	<0.001

ALB Albumin, *Wbc* White blood cell, *Rbc* Red blood cell, *Hb* Hemoglobin, *Plt* Platelet, *Ca199* Carbohydrate Antigen 199, *CEA* Carcinoembryonic Antigen, *AFP* Alpha-Fetoprotein, *Ca125* Carbohydrate Antigen 125

Performance evaluation of multiple ML models

Based on the nine selected features, we developed seven ML models, including LR, KNN, RF, XGBoost, DT, GBM, and SVM. The parameters of each model are presented in Table S3. To assess the classification performance of these models, several metrics were calculated using the confusion matrix from the training and internal validation cohort, including ROC AUC, accuracy, sensitivity, specificity, recall, F1 score, and Brier score (Table 3). A radar chart (Fig. 4) was also created to visually compare the multidimensional performance of the models, enhancing the interpretability of the results. Among these models, XGBoost demonstrated the best overall performance, achieving an ROC AUC of 0.901, accuracy of 0.846, sensitivity of 0.756, specificity of 0.897, recall of 0.756, and an F1 score of 0.82, outperforming all other models.

Additional performance comparisons were made using ROC curves, PR curves, calibration curves, and DCA. In the ROC analysis, the training cohort showed XGBoost achieved an AUC of 0.97 (Fig. 5A), while the validation cohort demonstrated an AUC of 0.901 (Fig. 5B), demonstrating its strong ability to differentiate between positive and negative samples. The training cohort PR curve analysis showed a precision-recall curve AUC of 0.943 (Fig. 5C), with the validation cohort maintaining 0.827 (Fig. 5D), emphasizing its ability to maintain a balance between precision and recall across various thresholds, thereby underscoring its classification reliability and stability. Calibration curves revealed excellent probability alignment in both training (Brier score 0.074, Fig. 5E) and validation (Brier score 0.12, Fig. 5F) cohorts. A lower Brier score reflects more accurate probability estimations, thereby increasing the model's credibility in clinical decision-making. DCA further revealed that XGBoost offered significantly higher net benefits across most threshold probability ranges compared to the other models (Fig. 5G, H). The learning curve analysis (Figure S3) confirmed stable model performance with a minimal accuracy gap of 0.049 between training and validation sets, effectively ruling out overfitting concerns. Based on these comprehensive analyses and visualized results, XGBoost was chosen as the core algorithm for constructing the final predictive model.

SHAP-Based interpretability for XGBoost

We employed SHAP visualizations to gain an in-depth understanding of the key features driving the model's predictions. The SHAP summary plot (Fig. 6A) illustrates both the direction and magnitude of each feature's contribution to the predicted outcomes. Positive values indicate a feature that increases the predicted probability, whereas negative values suggest a decrease in probability. The gradient colors reflect feature values, with yellow representing higher values and purple indicating lower values. For instance, SHAP values for PDAC patients with tumor emboli predominantly fall within the positive range, suggesting that tumor embolus is associated with an elevated probability of ELM. Conversely, SHAP values for PDAC patients who received adjuvant chemotherapy are mainly clustered in the negative range, indicating that such treatment may lower the likelihood of ELM. The SHAP bar plot (Fig. 6B) ranks features according to their average SHAP values, reflecting their relative importance in the model. Tumor embolus had the highest contribution, followed by N stage and adjuvant chemotherapy, underscoring their crucial roles in the prediction model. Fatty liver, tumor location, and differentiation were identified as moderately important factors. SHAP dependence plots (Fig. 6C) further depict the specific impact patterns of individual features on predicted outcomes. Each subplot represents a single feature, with the x-axis showing the feature value and the y-axis displaying the corresponding SHAP value. For example, for fatty liver, higher feature values correlated with lower SHAP values, suggesting that fatty liver may reduce the probability of ELM. Finally, we presented SHAP force plots for two individual cases. As illustrated in Fig. 6D, for a patient who developed ELM, the absence of tumor embolus and fatty liver, along with an N2 stage and G3-4 differentiation, collectively contributed to a prediction score significantly higher than the baseline ($E[f(x)] = -0.703$), yielding a final prediction value of 3.21. In contrast, for a patient without ELM, the prediction score was −2.03. These visualizations provide an intuitive understanding of each variable's role in the prediction, while also highlighting the model's sensitivity to variations in input variables.

Validation of the XGBoost model

A comprehensive evaluation was performed to assess the model's performance and clinical utility across multiple datasets. The AUC values for the training, internal validation, and external validation datasets were 0.97, 0.90, and 0.95, respectively, indicating consistent predictive performance across various datasets (Fig. 7A-C). As shown in Fig. 7D-F, the predicted probabilities of ELM generated by the XGBoost model closely matched the actual probabilities, approaching the ideal line in both the training and validation datasets. Calibration, validated through 1,000 bootstrap iterations, further demonstrated the high predictive accuracy of the model, especially in the low-to-moderate risk range, underscoring its reliable calibration. DCA analysis indicated that XGBoost consistently offered greater decision-making benefits for PDAC patients compared to a non-model-based approach across all three cohorts as risk thresholds increased (Fig. 7G-I). The CIC analysis further highlighted the substantial clinical benefit of XGBoost (Fig. 7J-L).

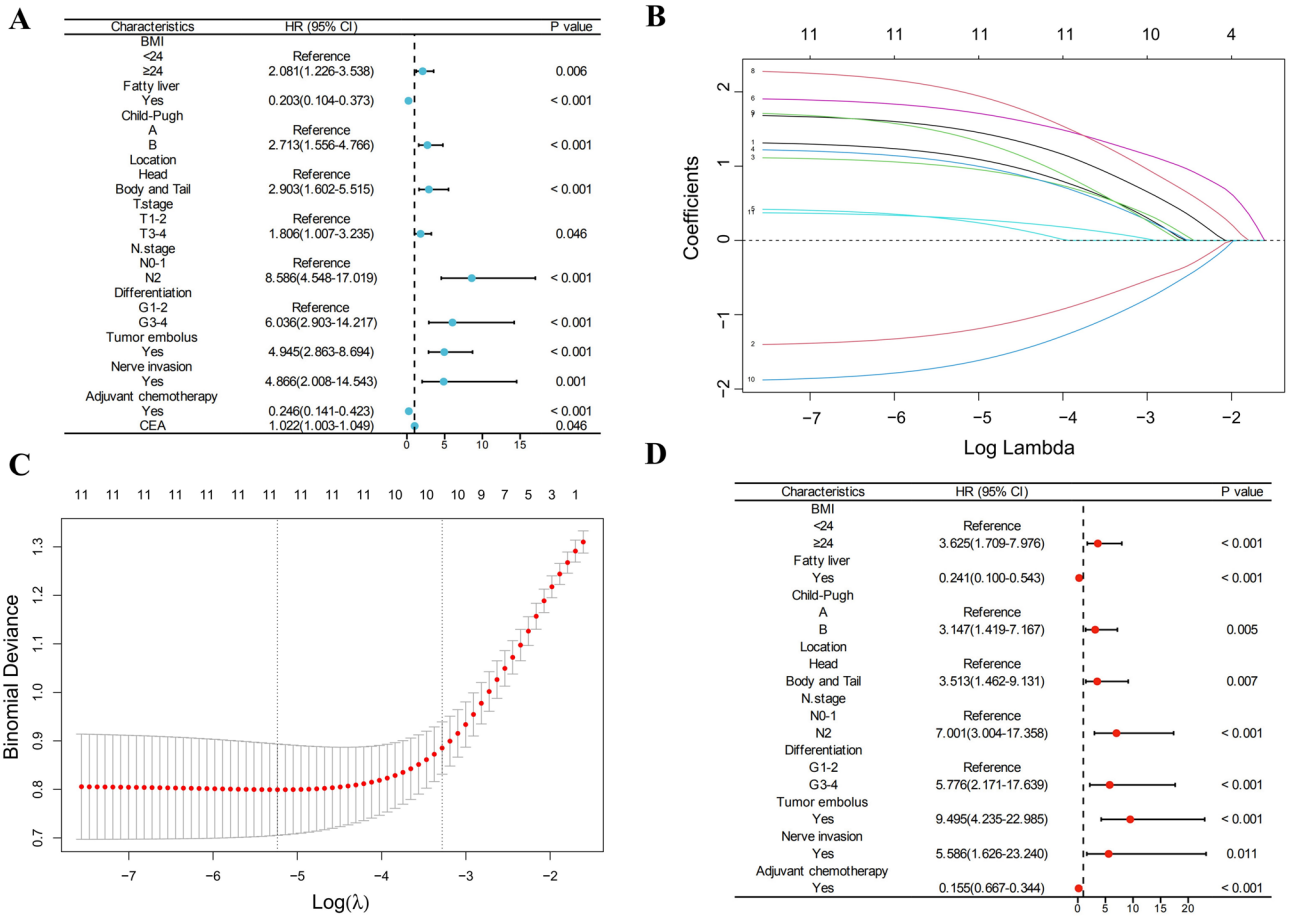

Fig. 2 Selection of feature variables for model construction: **A** Forest plot of univariate Cox regression for variable selection. **B** A graph showing the LASSO coefficient trajectories, and **C** a curve of cross-validation error representing the selection of the tuning parameter (λ). **D** Multivariate Cox regression forest plot to identify the final feature variables

Development of an online interactive calculator

The XGBoost model, built using nine indicators, was deployed on an online platform to enable personalized prediction of ELM in PDAC patients (Fig. 8). This tool is designed to provide theoretical guidance to support clinical decision-making. The model can be accessed via the following link: https://haozhu.shinyapps.io/liver-prediction/.

Discussion

The liver, with its abundant blood supply and unique microenvironment, is the most common site of metastasis for pancreatic cancer [17]. However, there is currently no universally accepted definition for ELM. Sugiura et al. proposed that liver metastasis occurring within six months after pancreatic cancer surgery should be considered ELM [18, 19], while the 2021 National Comprehensive Cancer Network (NCCN) guidelines defined the timeframe as within one year post-surgery [20]. In this study, we adopt the definition of ELM as occurring within one year after surgery. Regardless of the specific definition, early detection of liver metastasis is crucial for improving patient prognosis. With continuous advancements in imaging technologies and biomarkers, significant progress has been made in the early detection of liver metastasis in clinical practice [21, 22]. In recent years, the widespread application of ML and other artificial intelligence technologies has led to remarkable achievements across various fields. Therefore, this study employs ML algorithms to conduct comprehensive analyses using multi-factor models, aiming to accurately predict the occurrence of ELM after PDAC surgery, personalize treatment plans, improve survival rates, and reduce the treatment burden.

Xu et al. previously conducted univariate and multivariate regression analyses to select relevant variables, and developed a preoperative prediction model for recurrence and survival in PDAC patients based on these variables [23]. However, the study had several limitations. First, the study only included PDAC patients with tumors located in the pancreatic head, limiting its applicability to other patient populations. Second, the variables

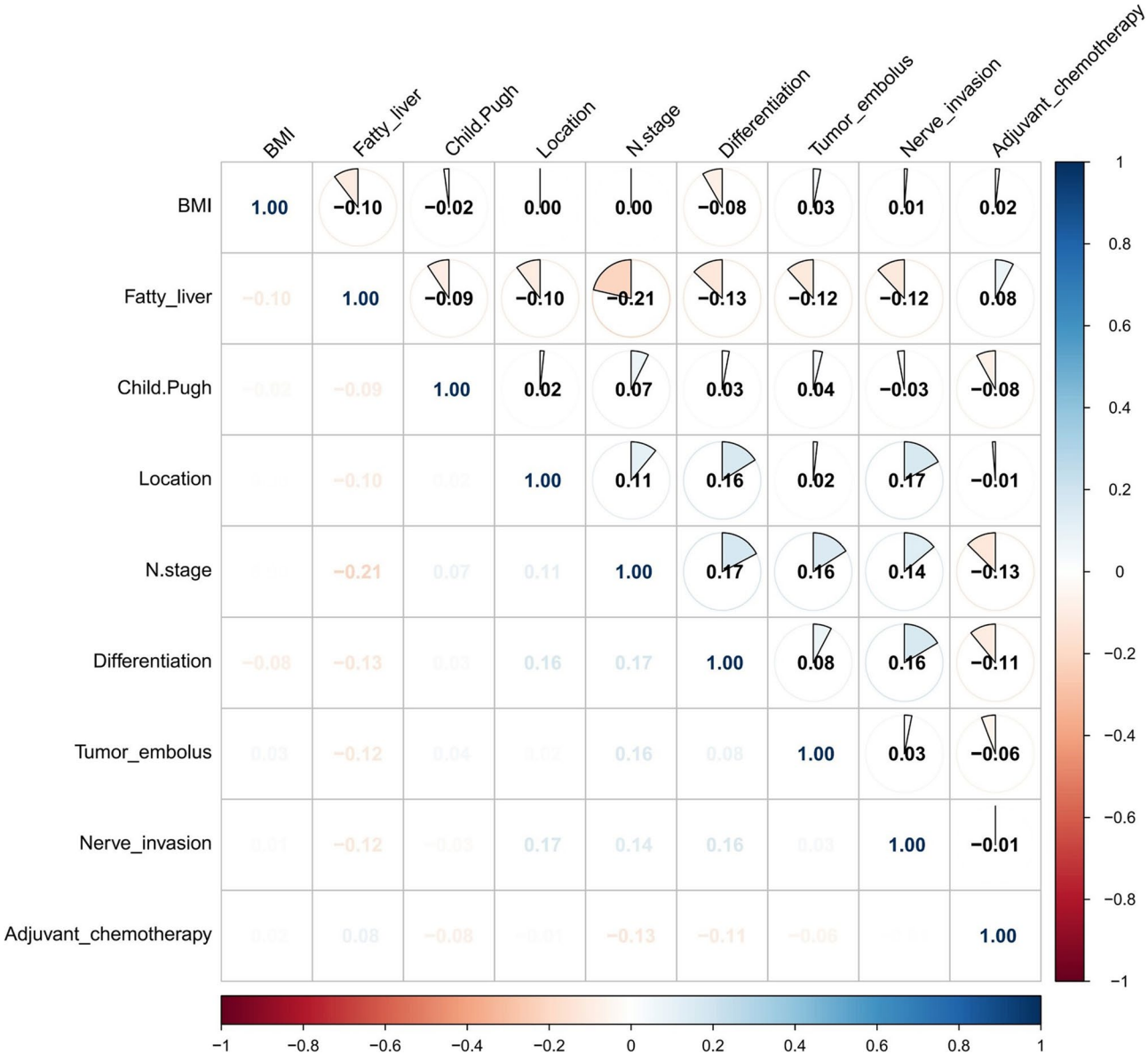

Fig. 3 Heatmap of the correlation among the nine variables used for model construction

Table 3 Comprehensive performance assessment of seven models

Model	AUROC	Accuracy	Sensitivity	Specificity	Recall	F1_Score	Brier_Score
XGBoost	0.9014	0.8455	0.7556	0.8974	0.7556	0.8204	0.1200
Logistic Regression	0.8843	0.7967	0.6889	0.8590	0.6889	0.7646	0.1380
KNN	0.8882	0.7886	0.6222	0.8846	0.6222	0.7306	0.1340
Random Forest	0.8791	0.7967	0.6667	0.8718	0.6667	0.7556	0.1370
Decision Tree	0.7358	0.7236	0.6444	0.7692	0.6444	0.7013	0.1920
GBM	0.8840	0.8130	0.6889	0.8846	0.6889	0.7746	0.1380
SVM	0.8778	0.7967	0.6444	0.8846	0.6444	0.7457	0.1420

considered in the model were restricted to preoperative examination results, without incorporating pathological data that could more accurately reflect tumor characteristics. Finally, the model was based exclusively on three variables—Ca199, preoperative pain symptoms, and the fibrinogen-to-albumin ratio (FAR)—which may lack sufficient representativeness and limit the model's external validity. Furthermore, another retrospective study employed the XGBoost algorithm to develop a model for predicting PDAC mortality outcomes, achieving

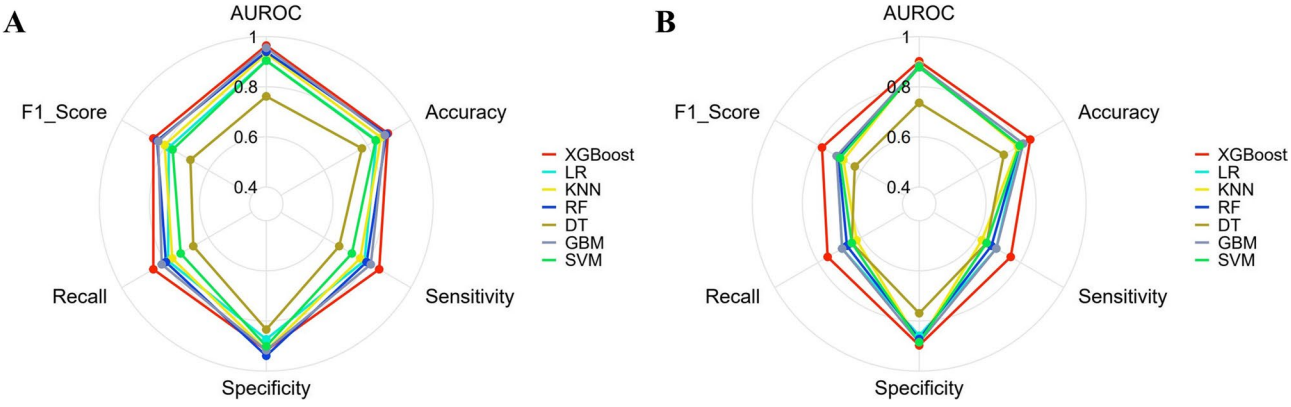

Fig. 4 Radar chart comparison of seven machine learning models' performance metrics in (**A**) training and (**B**) validation cohorts

an impressive AUC of 0.933 [24]. However, the authors did not offer sufficient model interpretability or create a clinical platform, limiting its practical utility in clinical settings. The advantage of this study lies in its pioneering use of a local database combined with ML methods to predict ELM in PDAC, an area currently lacking similar research. Secondly, the study incorporated a comprehensive set of features, particularly tumor pathological characteristics, which enhanced both the reliability and predictive performance of the model. In the final stage, we collaborated with an external validation group, a decision driven by a deep awareness of the limitations and potential biases associated with relying on a single research institution. This strategy aimed to not only enhance the reliability of the study's conclusions but also to establish a robust theoretical foundation for their broader applicability and generalizability across diverse clinical settings.

In our study, tumor embolus was identified as the most significant factor in the final prediction model. Tumor emboli are formed within the tumor system and contribute to vascular occlusion [25]. Previous research has demonstrated that tumor emboli adversely affect the prognosis of several cancers, including colorectal cancer and non-metastatic clear cell renal cell carcinoma [26]. The formation of tumor emboli involves both the physical aggregation of tumor cells and the activation of coagulation pathways, along with the initiation of immune evasion mechanisms. On one hand, highly invasive tumor cells stimulate the formation of cancer emboli by secreting procoagulant substances, such as tissue factor and procoagulant microparticles [27]. On the other hand, the interaction between tumor cells and platelets stabilizes tumor emboli more effectively than ordinary blood clots, and this blastocyst-like structure aids in immune evasion by tumor cells [28]. Additionally, calpain-mediated hydrolysis of E-cadherin within tumor emboli plays a critical role in sustaining tumor cell activity and promoting distant metastasis, which may contribute to chemoresistance and enhanced metastatic potential [29]. At present, gemcitabine combined with albumin-bound paclitaxel (GA) or FOLFIRINOX is established as the first-line chemotherapy regimen for PDAC, offering potential long-term survival benefits [30]. However, the selection of a chemotherapy regimen should be personalized based on the individual patient's characteristics. According to Dosso et al., FOLFIRINOX demonstrates superior efficacy in patients with an Eastern Cooperative Oncology Group (ECOG) performance status (PS) of 0–1, good overall health, age < 65 years, and normal liver function. In contrast, GA may be a more suitable option for elderly patients, those with multiple comorbidities, or those with poor therapy tolerance [31]. In this study, higher Child-Pugh scores, overweight status, and fatty liver were found to be independent risk factors for ELM. These findings imply that high-risk patients for ELM might benefit more from GA, considering its relatively less favorable tolerability profile. However, this hypothesis requires further validation to confirm its clinical utility in guiding chemotherapy regimen selection. Furthermore, it is important to note that some studies have reported that low doses of gemcitabine may paradoxically promote pancreatic cancer metastasis. This unexpected finding emphasizes the necessity of careful dose management and underscores the importance of prudent decision-making in the clinical use of gemcitabine [32].

The prevailing consensus suggests that fatty liver may influence cancer development and metastasis via multiple mechanisms. However, significant debate exists among researchers concerning whether fatty liver promotes or inhibits cancer progression. A cohort study involving 8 million individuals revealed that patients with non-alcoholic fatty liver disease (NAFLD) had a significantly elevated risk of pancreatic cancer during follow-up (HR: 1.17, 95% CI: 1.09–1.26), with a progressive increase in risk corresponding to higher fatty liver index values [33]. Furthermore, several studies have demonstrated a significant positive correlation between NAFLD and liver

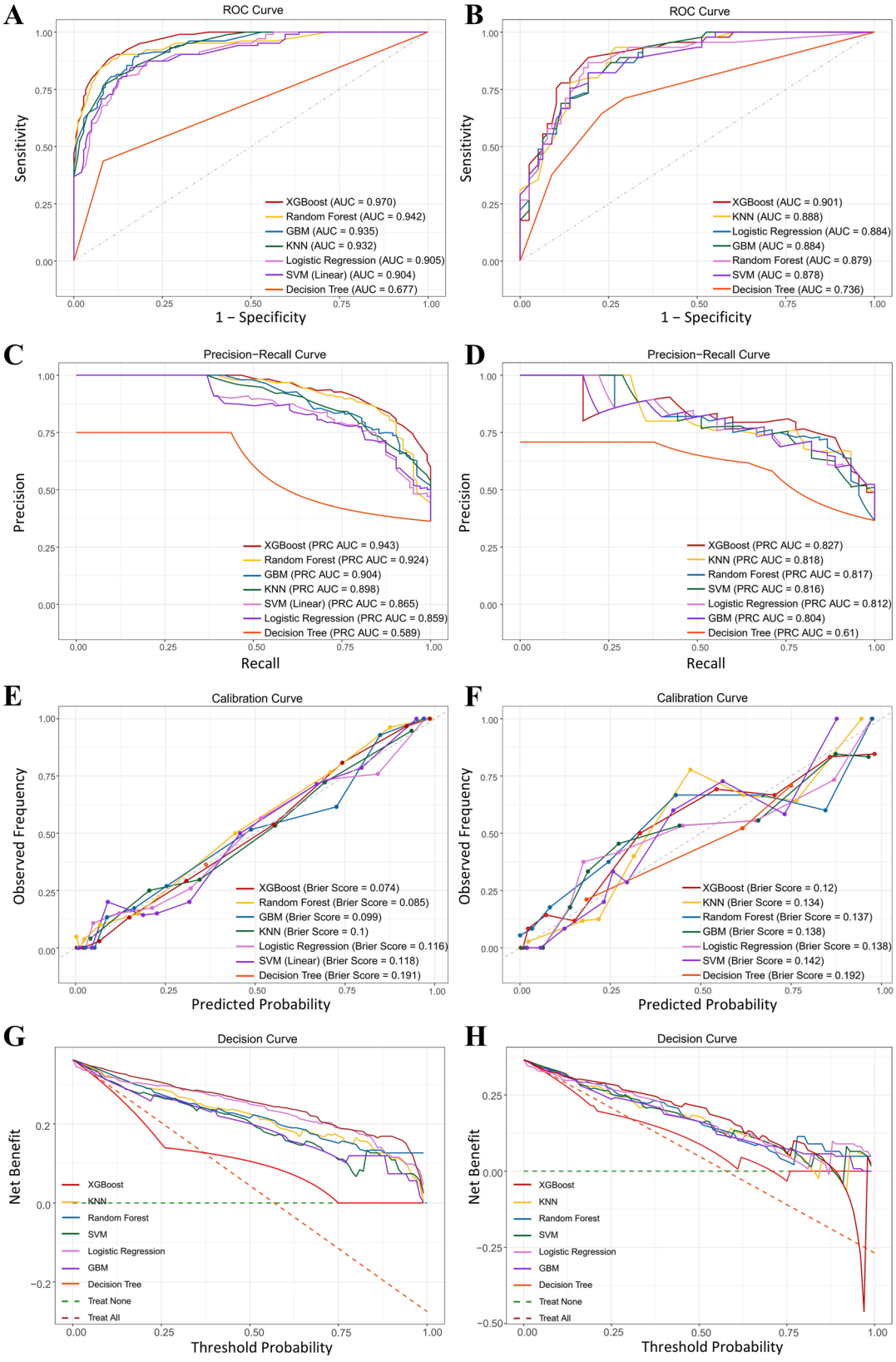

Fig. 5 To assess the predictive ability of the seven machine learning models in the training and validation cohort, we utilized various evaluation tools including the ROC curve (**A**)(**B**), PRC (**C**)(**D**), calibration plot (**E**)(**F**), and DCA plot (**G**)(**H**)

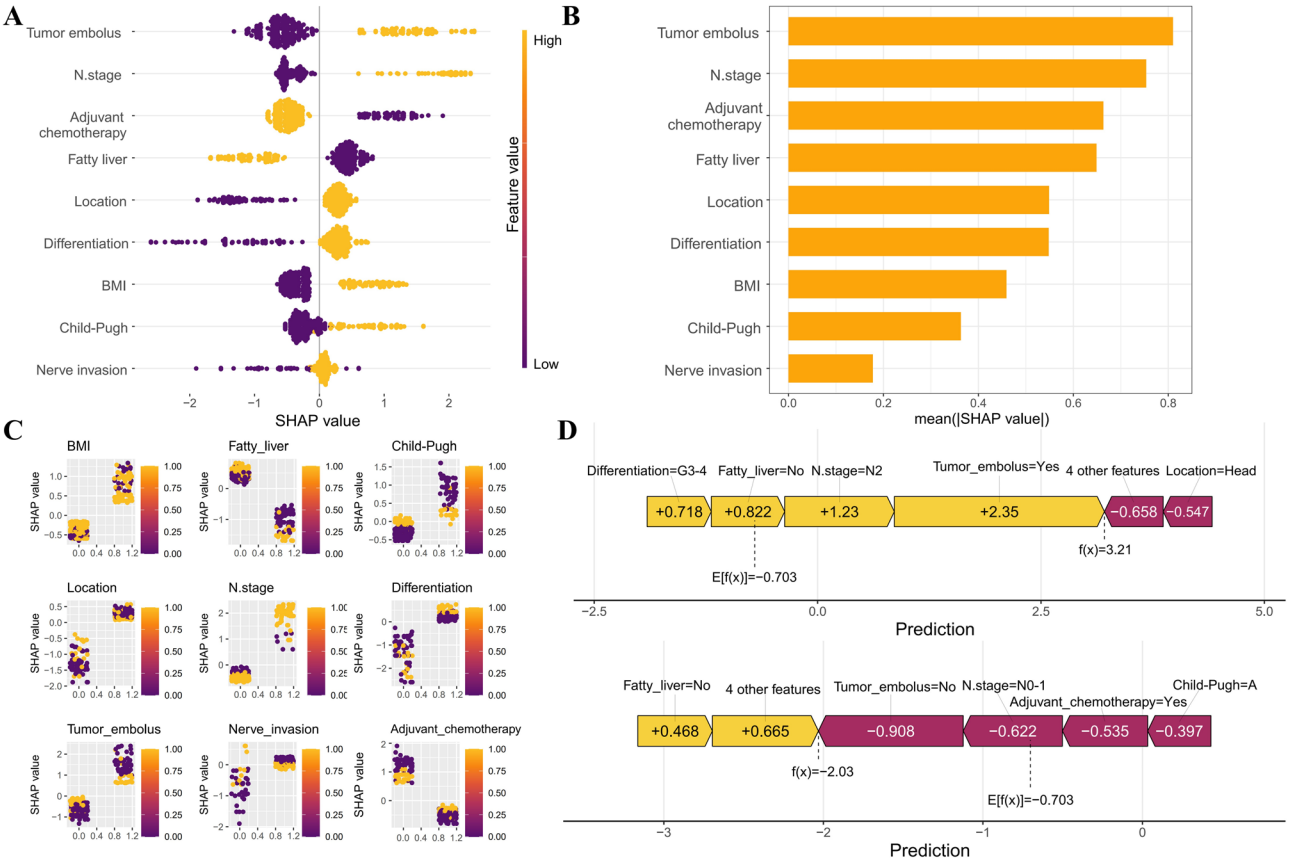

Fig. 6 The Shapley Additive Explanations method was used to interpret the XGBoost model. **A** SHAP Summary Plot, where both positive and negative SHAP values indicate how each feature either increases or decreases the predicted outcome. **B** SHAP Bar Plot displays the average absolute SHAP values for each feature, highlighting the most important features in the model. Longer bars represent greater feature importance. **C** SHAP dependence plots show the relationship between predicted risk and feature values, illustrating how different value ranges influence the predictions. **D** Individual sample force plots for ELM and non-ELM patients, demonstrating the impact of each feature on their respective outcomes

metastasis of colorectal cancer. This is attributed to the upregulation of fatty acid synthase (FASN) within the lipid-rich microenvironment of NAFLD, which promotes palmitic acid synthesis in metastatic colorectal cancer (CRC) cells, aiding their colonization and spread in liver tissue [34, 35]. In contrast, two other studies reported entirely contradictory findings: colorectal cancer patients with fatty liver showed a significantly reduced likelihood of liver metastasis [36, 37]. Similarly, a retrospective study by Wu et al. found that breast cancer patients with fatty liver experienced significantly earlier liver metastasis compared to those without fatty liver ($p = 0.022$) [38]. In alignment with this, the SHAP summary plot from this study indicates that PADC combined with fatty liver exerts a significant protective effect against ELM. These conflicting perspectives raise important questions. Our team has undertaken a comprehensive analysis of this phenomenon, recognizing that the development of fatty liver is associated with several physiological changes, including insulin resistance, obesity, dyslipidemia, and increased levels of inflammatory markers. These changes, on one hand, impair the body's immune response, while on the other hand, promote the overexpression of oncogenes [39]. Consequently, the hypothesis that fatty liver increases the likelihood of cancer development is plausible. However, tumor metastasis differs fundamentally from tumor development. In the metastatic process, only a small subset of tumor cells can breach barriers and successfully form new tumor nodules in distant tissues [40]. This process is influenced not only by the tumor's ability to invade tissues but also by the biological microenvironment of the metastatic target organ. Fatty liver may partially inhibit the growth of liver metastatic tumors by suppressing angiogenesis and reducing the activity of pyrimidine nucleoside phosphorylase [41]. Moreover, animal experiments have shown that the growth of colon cancer metastatic tumors in the livers of mice with high dietary fatty acid intake is significantly reduced [42]. This could be a key factor explaining why fatty liver acts as a protective factor against liver metastasis in certain malignancies. Nevertheless, our stance does not endorse a high-fatty acid diet; we maintain that regular eating

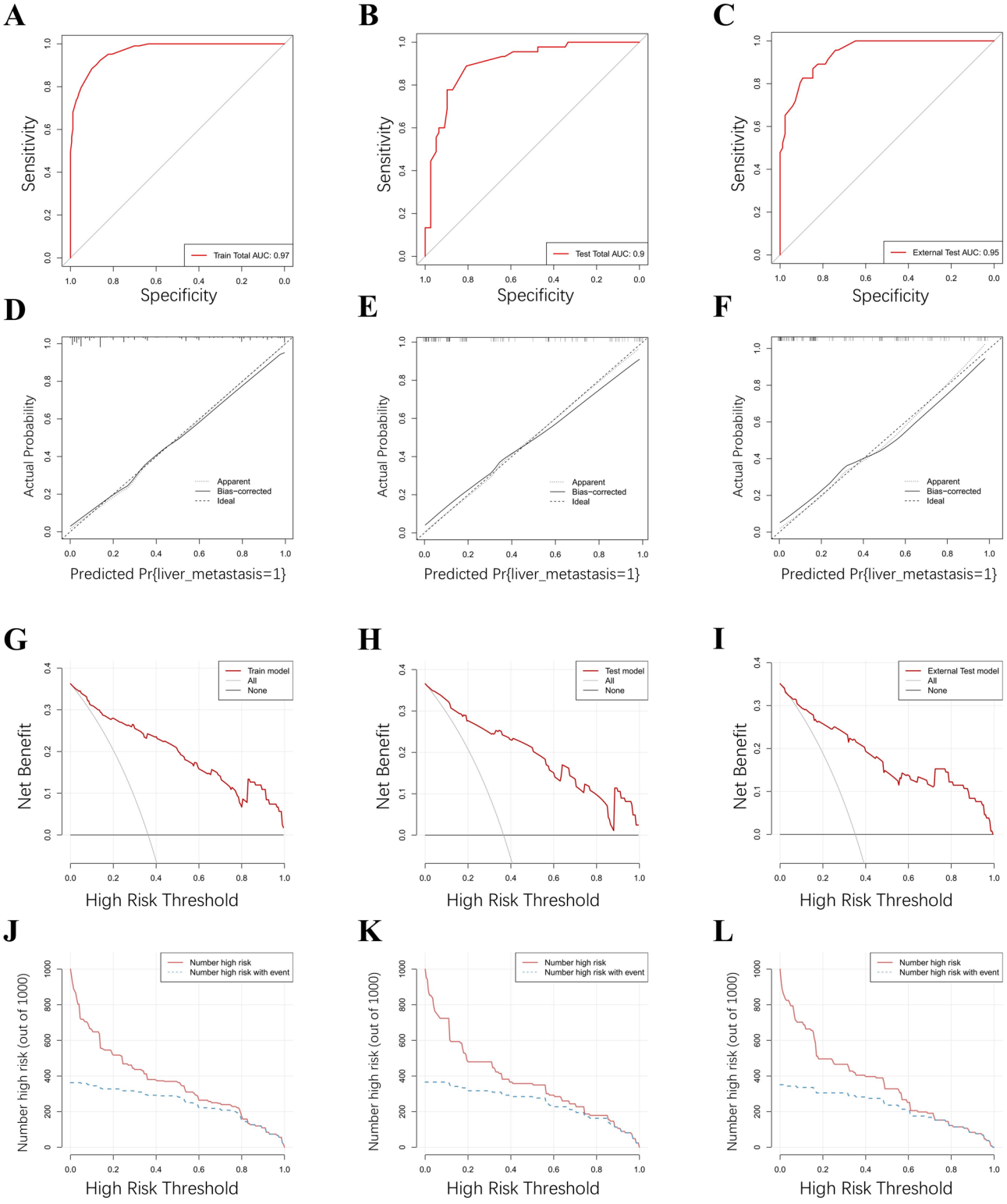

Fig. 7 Validation of the model in each cohort to assess its generalizability. ROC curves for the training cohort (**A**), internal validation cohort (**B**) and external validation cohort (**C**). **D**, **E**, and **F** Calibration curves for the model in the training, internal validation, and external validation cohorts, respectively, illustrating the agreement between predicted and observed outcomes. **G**, **H**, and **I** DCA curves for the three cohorts, evaluating the clinical utility of the model in each group. **J**, **K**, and **L** CIC curves for the three cohorts, further assessing the clinical effectiveness of the model across the different groups

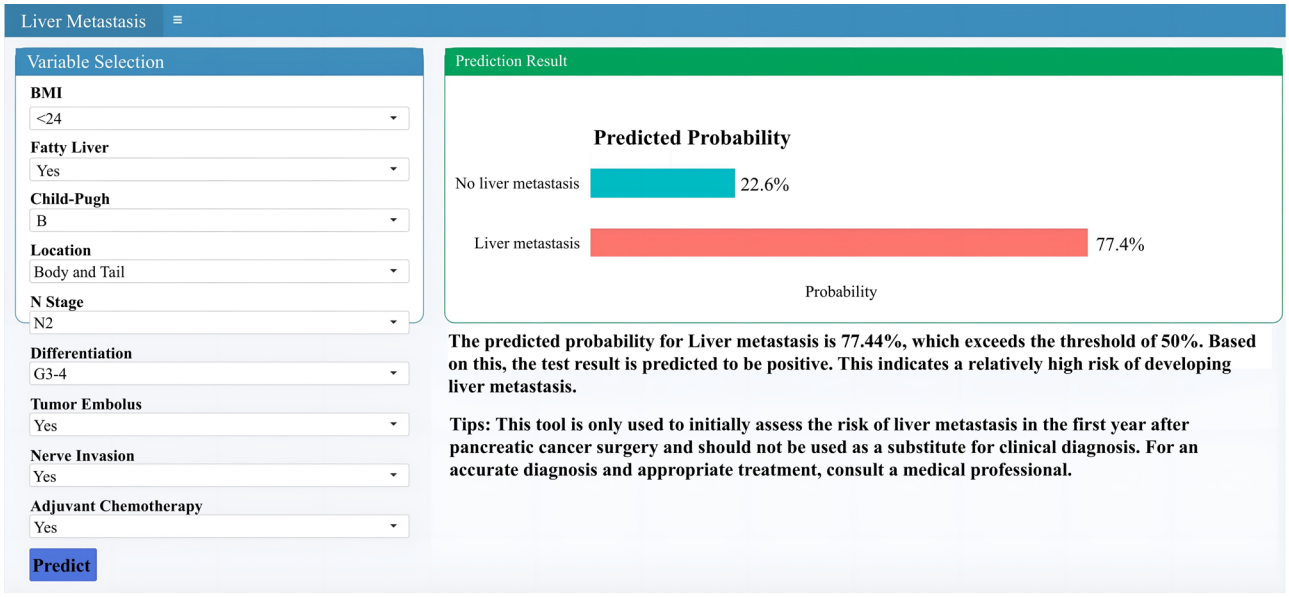

Fig. 8 Deployment of the XGBoost prediction model for early liver metastasis of pancreatic cancer onto the internet

habits and a balanced diet are more beneficial to overall health.

Previous studies have established that tumors in the pancreatic body and tail are more prone to metastatic disease than those in the pancreatic head, a finding consistent with our own research [43]. We propose that when pancreatic head tumors reach a certain size, they cause mechanical obstruction of the bile duct, resulting in bile stasis and the onset of obstructive jaundice. This often leads to early patient examination and intervention, a phenomenon less commonly observed in pancreatic body and tail tumors. Kazuaki et al. reported that infiltration of para-aortic lymph nodes serves as an independent predictor of postoperative recurrence [44]. However, the area surrounding the pancreatic head predominantly consists of aortic neural networks [45], which makes lymphatic infiltration less likely and, consequently, delays recurrence. Nonetheless, this hypothesis may require further clinical and pathological investigations for validation.

Bojmar et al. noted that although the liver may not be directly involved at the time of surgery for PDAC patients, cancer, as a systemic disease, affects the entire body, extending beyond local tissues. As the liver plays a central role in most physiological functions, it is essential to adopt a systemic perspective when understanding the pathological processes and treatment strategies for cancer [46]. Originally, the Child-Pugh score was developed to assess the long-term prognosis of chronic liver disease patients by indicating liver function stability. Currently, this score is extensively used in various areas, including preoperative evaluation and drug dosage adjustment [47]. Consequently, this study incorporated the Child-Pugh score to assess liver function and damage in PDAC patients, providing a systematic and dynamic evaluation of factors related to ELM. Our model included factors such as N stage, tumor differentiation, and nerve invasion, as anticipated. However, T stage was excluded from the model, likely due to the small sample size, which may have obscured the impact of tumor size on ELM. Moreover, while tumor size correlates with prognosis, the aggressive nature of pancreatic cancer means that even tumors with smaller diameters are associated with poor outcomes for a substantial proportion of patients. This is likely because smaller tumors often exhibit microvascular invasion characteristics akin to those found in larger tumors [48].

Our study has several limitations. First, due to the inherent limitations of retrospective studies, baseline data inevitably contains missing values. To mitigate this, we employed the KNN method for data imputation to reduce potential biases in the results. However, the effectiveness of this approach may still be constrained. Second, while PDAC cases were collected from two major medical centers, the sample size remains insufficient for robust ML modeling. Future studies will require multicenter, large-scale cohorts to improve the model's accuracy. Third, our exclusion of patients who received neoadjuvant therapy may limit the model's generalizability to this important subgroup of pancreatic cancer patients, particularly as neoadjuvant approaches are increasingly adopted in clinical practice. Fourth, the lack of standardized documentation regarding resectability status (resectable vs. borderline resectable) in our retrospective cohort may affect readers' ability to fully contextualize our findings within the spectrum of surgical

candidates. Additionally, although we included postoperative chemotherapy as a variable, the heterogeneity in chemotherapy regimens among patients may influence the model's predictive accuracy. Therefore, exploring strategies to optimize chemotherapy regimens based on individual patient characteristics remains a critical avenue for future research.

Conclusion

Our study developed an interpretable predictive model that significantly enhances the prediction of postoperative ELM in PDAC patients and deployed this model online, offering clinicians an intuitive and convenient tool. This tool provides vital decision-making support for clinicians in tailoring personalized treatment plans, thereby contributing to the advancement of precision medicine.

Supplementary Information

The online version contains supplementary material available at https://doi.org/10.1186/s12885-025-14503-3.

Supplementary Material 1. Fig. S1. (A) Bar plot showing the percentage of missing values for each of the 23 features. (B) Yellow squares represent missing values.

Supplementary Material 2. Fig. S2. Multicollinearity analysis excluding variables with VIF > 5 (A) or tolerance < 0.1(B).

Supplementary Material 3. Fig. S3. The learning curve demonstrates the model's performance across increasing training sample sizes in both the training and validation cohorts.

Supplementary Material 4. Table S1.Clinical characteristics of patients in the training and internal validation cohorts.

Supplementary Material 5. Table S2. The Lasso coefficients of each feature.

Supplementary Material 6. Table S3. Parameters of the Seven Models.

Acknowledgements

No.

Authors' contributions

The study was devised and planned by H.Z, D.S and DY.S. H.Z wrote the manuscript. YY.Z, KJ.W, XJ.G, XF.X collected the PDAC patients clinical data, and completed the follow-up examinations of PDAC patients after surgery. H.Z, WG.Z, XH.Y, JY.Q carried out data analysis. D.S ultimately reviewed and revised the manuscript. All authors approved the final manuscript.

Funding

This study was supported by the National Nature Science Foundation of China (No. 82203735), the Gusu Health Talent Program (No. GSWS2022026), and Pilot Project of Suzhou Basic Research (SSD2024068). This work was also supported by the Pilot Project of Suzhou Basic Research (SSD2024068 to Xiaojie Gan).

Data availability

The data analyzed during the current study are available from the first author upon reasonable request.

Declarations

Ethics approval and consent to participate

This study complies with the guidelines of the Helsinki Declaration and has been approved by the Ethics Committee of the First Affiliated Hospital of Soochow University and the Affiliated Hospital of Nantong University. All research procedures are in accordance with relevant laws. Informed consent from patients is waived due to the collection of only clinically relevant patient data.

Consent for publication

Not applicable.

Competing interests

The authors declare no competing interests.

Received: 28 January 2025 / Accepted: 12 June 2025
Published online: 01 July 2025

References

1. Saloman JL, Albers KM, Li D, Hartman DJ, Crawford HC, Muha EA, et al. Ablation of sensory neurons in a genetic model of pancreatic ductal adenocarcinoma slows initiation and progression of cancer. Proc Natl Acad Sci U S A. 2016;113:3078–83. https://doi.org/10.1073/pnas.1512603113.
2. Kisling SG, Natarajan G, Pothuraju R, Shah A, Batra SK, Kaur S. Implications of prognosis-associated genes in pancreatic tumor metastasis: lessons from global studies in bioinformatics. Cancer Metastasis Rev. 2021;40:721–38. https://doi.org/10.1007/s10555-021-09991-1.
3. Rahib L, Smith BD, Aizenberg R, Rosenzweig AB, Fleshman JM, Matrisian LM. Projecting cancer incidence and deaths to 2030: the unexpected burden of thyroid, liver, and pancreas cancers in the United States. Cancer Res. 2014;74:2913–21. https://doi.org/10.1158/0008-5472.Can-14-0155.
4. Davalos V, Esteller M. Cancer epigenetics in clinical practice. CA Cancer J Clin. 2023;73:376–424. https://doi.org/10.3322/caac.21765.
5. Bosetti C, Rosato V, Li D, Silverman D, Petersen GM, Bracci PM, et al. Diabetes, antidiabetic medications, and pancreatic cancer risk: an analysis from the international pancreatic cancer case-control consortium. Ann Oncol. 2014;25:2065–72. https://doi.org/10.1093/annonc/mdu276.
6. van Roessel S, Kasumova GG, Verheij J, Najarian RM, Maggino L, de Pastena M, et al. International validation of the eighth edition of the American Joint Committee on Cancer (AJCC) TNM staging system in patients with resected pancreatic cancer. JAMA Surg. 2018;153:e183617. https://doi.org/10.1001/jamasurg.2018.3617.
7. Bertsimas D, Wiberg H. Machine learning in oncology: methods, applications, and challenges. JCO Clin Cancer Inf. 2020;4:885–94. https://doi.org/10.1200/cci.20.00072.
8. Zhong X, Lin Y, Zhang W, Bi Q. Predicting diagnosis and survival of bone metastasis in breast cancer using machine learning. Sci Rep. 2023;13:18301. https://doi.org/10.1038/s41598-023-45438-z.
9. Li L, Pu C, Jin N, Zhu L, Hu Y, Cascone P, et al. Prediction of 5-year overall survival of tongue cancer based machine learning. BMC Oral Health. 2023;23:567. https://doi.org/10.1186/s12903-023-03255-w.
10. Wang Q, Qiao W, Zhang H, Liu B, Li J, Zang C, et al. Nomogram established on account of Lasso-Cox regression for predicting recurrence in patients with early-stage hepatocellular carcinoma. Front Immunol. 2022;13:1019638. https://doi.org/10.3389/fimmu.2022.1019638.
11. Rudin C. Stop explaining black box machine learning models for high stakes decisions and use interpretable models instead. Nat Mach Intell. 2019;1:206–15. https://doi.org/10.1038/s42256-019-0048-x.
12. Muhammad D, Bendechache M. Unveiling the black box: a systematic review of explainable artificial intelligence in medical image analysis. Comput Struct Biotechnol J. 2024;24:542–60. https://doi.org/10.1016/j.csbj.2024.08.005.
13. Lundberg SM, Erion G, Chen H, DeGrave A, Prutkin JM, Nair B, et al. From local explanations to global understanding with explainable AI for trees. Nat Mach Intell. 2020;2:56–67. https://doi.org/10.1038/s42256-019-0138-9.
14. Zou J, Chen H, Liu C, Cai Z, Yang J, Zhang Y, et al. Development and validation of a nomogram to predict the 30-day mortality risk of patients with intracerebral hemorrhage. Front Neurosci. 2022;16:942100. https://doi.org/10.3389/fnins.2022.942100.
15. Han Y, Wang S. Disability risk prediction model based on machine learning among Chinese healthy older adults: results from the China health and retirement longitudinal study. Front Public Health. 2023;11:1271595. https://doi.org/10.3389/fpubh.2023.1271595.
16. Kerr KF, Brown MD, Zhu K, Janes H. Assessing the clinical impact of risk prediction models with decision curves: guidance for correct interpretation and

appropriate use. J Clin Oncol. 2016;34:2534–40. https://doi.org/10.1200/jco.2015.65.5654.
17. Fabian A, Stegner S, Miarka L, Zimmermann J, Lenk L, Rahn S, et al. Metastasis of pancreatic cancer: an uninflamed liver micromilieu controls cell growth and cancer stem cell properties by oxidative phosphorylation in pancreatic ductal epithelial cells. Cancer Lett. 2019;453:95–106. https://doi.org/10.1016/j.canlet.2019.03.039.
18. Sugiura T, Uesaka K, Kanemoto H, Mizuno T, Sasaki K, Furukawa H, et al. Serum CA19-9 is a significant predictor among preoperative parameters for early recurrence after resection of pancreatic adenocarcinoma. J Gastrointest Surg. 2012;16:977–85. https://doi.org/10.1007/s11605-012-1859-9.
19. Matsumoto I, Murakami Y, Shinzeki M, Asari S, Goto T, Tani M, et al. Proposed preoperative risk factors for early recurrence in patients with resectable pancreatic ductal adenocarcinoma after surgical resection: a multi-center retrospective study. Pancreatology. 2015;15:674–80. https://doi.org/10.1016/j.pan.2015.09.008.
20. Tempero MA, Malafa MP, Al-Hawary M, Behrman SW, Benson AB, Cardin DB, et al. Pancreatic adenocarcinoma, version 2.2021, NCCN clinical practice guidelines in oncology. J Natl Compr Canc Netw. 2021;19:439–57. https://doi.org/10.6004/jnccn.2021.0017.
21. Lu W, Wu G, Miao X, Ma J, Wang Y, Xu H, et al. The radiomics nomogram predicts the prognosis of pancreatic cancer patients with hepatic metastasis after chemoimmunotherapy. Cancer Immunol Immunother. 2024;73:183. https://doi.org/10.1007/s00262-024-03739-w.
22. Xie Z, Gao Y, Ho C, Li L, Jin C, Wang X, et al. Exosome-delivered CD44v6/C1QBP complex drives pancreatic cancer liver metastasis by promoting fibrotic liver microenvironment. Gut. 2022;71:568–79. https://doi.org/10.1136/gutjnl-2020-323014.
23. Xu S, Zhang XP, Zhao GD, Zou WB, Zhao ZM, Liu Q, et al. Derivation and validation of a preoperative prognostic model for resectable pancreatic ductal adenocarcinoma. Hepatobiliary Pancreat Dis Int. 2023;22:160–8. https://doi.org/10.1016/j.hbpd.2022.09.009.
24. Nopour R. Establishment of prediction model for mortality risk of pancreatic cancer: a retrospective study. BMC Med Inf Decis Mak. 2024;24:181. https://doi.org/10.1186/s12911-024-02590-4.
25. Tathireddy H, Rice D, Martens K, Shivakumar S, Shatzel J. Breaking down tumor thrombus: current strategies for medical management. Thromb Res. 2023;230:144–51. https://doi.org/10.1016/j.thromres.2023.09.004.
26. Wu JH, Tian XY, Hao CY. The significance of a group of molecular markers and clinicopathological factors in identifying colorectal liver metastasis. Hepatogastroenterology. 2011;58:1182–8. https://doi.org/10.5754/hge11380.
27. Peng Q, Zhu J, Zhang Y, Jing Y. Blood hypercoagulability and thrombosis mechanisms in cancer patients -a brief review. Heliyon. 2024;10:e38831. https://doi.org/10.1016/j.heliyon.2024.e38831.
28. Mehta P. Potential role of platelets in the pathogenesis of tumor metastasis. Blood. 1984;63:55–63.
29. Ye Y, Tian H, Lange AR, Yearsley K, Robertson FM, Barsky SH. The genesis and unique properties of the lymphovascular tumor embolus are because of calpain-regulated proteolysis of E-cadherin. Oncogene. 2013;32:1702–13. https://doi.org/10.1038/onc.2012.180.
30. Santucci J, Tacey M, Thomson B, Michael M, Wong R, Shapiro J, et al. Impact of first-line FOLFIRINOX versus gemcitabine/Nab-paclitaxel chemotherapy on survival in advanced pancreatic cancer: evidence from the prospective international multicentre PURPLE pancreatic cancer registry. Eur J Cancer. 2022;174:102–12. https://doi.org/10.1016/j.ejca.2022.06.042.
31. De Dosso S, Siebenhüner AR, Winder T, Meisel A, Fritsch R, Astaras C, et al. Treatment landscape of metastatic pancreatic cancer. Cancer Treat Rev. 2021;96: 102180. https://doi.org/10.1016/j.ctrv.2021.102180.
32. Chen Y, Liu H, Zheng Q, Li H, You H, Feng Y, et al. Promotion of tumor progression induced by continuous low-dose administration of antineoplastic agent gemcitabine or gemcitabine combined with cisplatin. Life Sci. 2022;306:120826. https://doi.org/10.1016/j.lfs.2022.120826.
33. Park JH, Hong JY, Han K, Kang W, Park JK. Increased risk of pancreatic cancer in individuals with non-alcoholic fatty liver disease. Sci Rep. 2022;12:10681. https://doi.org/10.1038/s41598-022-14856-w.
34. Miyata T, Shinden Y, Motoyama S, Sannomiya Y, Tamezawa H, Nagayama T, et al. Non-alcoholic fatty liver disease may be a risk factor for liver metastasis after radical surgery for colorectal cancer: a retrospective study. J Gastrointest Cancer. 2024;55:932–9. https://doi.org/10.1007/s12029-024-01042-6.
35. Zhang C, Zhang Y, Dong Y, Zi R, Wang Y, Chen Y, et al. Non-alcoholic fatty liver disease promotes liver metastasis of colorectal cancer via fatty acid synthase dependent EGFR palmitoylation. Cell Death Discov. 2024;10:41. https://doi.org/10.1038/s41420-023-01770-x.
36. Murono K, Kitayama J, Tsuno NH, Nozawa H, Kawai K, Sunami E, et al. Hepatic steatosis is associated with lower incidence of liver metastasis from colorectal cancer. Int J Colorectal Dis. 2013;28:1065–72. https://doi.org/10.1007/s00384-013-1656-2.
37. Hayashi S, Masuda H, Shigematsu M. Liver metastasis rare in colorectal cancer patients with fatty liver. Hepatogastroenterology. 1997;44:1069–75.
38. Wu W, Chen J, Ye W, Li X, Zhang J. Fatty liver decreases the risk of liver metastasis in patients with breast cancer: a two-center cohort study. Breast Cancer Res Treat. 2017;166:289–97. https://doi.org/10.1007/s10549-017-4411-5.
39. Muzurović E, Mikhailidis DP, Mantzoros C. Non-alcoholic fatty liver disease, insulin resistance, metabolic syndrome and their association with vascular risk. Metabolism. 2021;119:154770. https://doi.org/10.1016/j.metabol.2021.154770.
40. Chambers AF, Groom AC, MacDonald IC. Dissemination and growth of cancer cells in metastatic sites. Nat Rev Cancer. 2002;2:563–72. https://doi.org/10.1038/nrc865.
41. Karube H, Masuda H, Hayashi S, Ishii Y, Nemoto N. Fatty liver suppressed the angiogenesis in liver metastatic lesions. Hepatogastroenterology. 2000;47:1541–5.
42. Gutt CN, Brinkmann L, Mehrabi A, Fonouni H, Müller-Stich BP, Vetter G, et al. Dietary omega-3-polyunsaturated fatty acids prevent the development of metastases of colon carcinoma in rat liver. Eur J Nutr. 2007;46:279–85. https://doi.org/10.1007/s00394-007-0662-y.
43. Paye F, Micelli Lupinacci R, Bachellier P, Boher JM, Delpero JR. Distal pancreatectomy for pancreatic carcinoma in the era of multimodal treatment. Br J Surg. 2015;102:229–36. https://doi.org/10.1002/bjs.9708.
44. Shimada K, Sakamoto Y, Sano T, Kosuge T. The role of paraaortic lymph node involvement on early recurrence and survival after macroscopic curative resection with extended lymphadenectomy for pancreatic carcinoma. J Am Coll Surg. 2006;203:345–52. https://doi.org/10.1016/j.jamcollsurg.2006.05.289.
45. Mitsunaga S, Hasebe T, Kinoshita T, Konishi M, Takahashi S, Gotohda N, et al. Detail histologic analysis of nerve plexus invasion in invasive ductal carcinoma of the pancreas and its prognostic impact. Am J Surg Pathol. 2007;31:1636–44. https://doi.org/10.1097/PAS.0b013e318065bfe6.
46. Roth S, Michalski C, Hoheisel JD. A systemic look at pancreatic cancer patients: predicting metastasis by studying the liver. Signal Transduct Target Ther. 2024;9: 246. https://doi.org/10.1038/s41392-024-01964-4.
47. Zhai Y, Hai D, Zeng L, Lin C, Tan X, Mo Z, et al. Artificial intelligence-based evaluation of prognosis in cirrhosis. J Transl Med. 2024;22:933. https://doi.org/10.1186/s12967-024-05726-2.
48. Izumi S, Nakamura S, Mano S, Onoda Y. Well-differentiated pancreatic ductal adenocarcinomas measuring ≤ 1 cm exhibit early features of tumor progression: a report of five lesions and a comparative study with advanced lesions. Surg Today. 2014;44:2058–64. https://doi.org/10.1007/s00595-013-0804-1.

Publisher's note